Received: 11 November 2022 | Revised: 2 February 2023 | Accepted: 15 February 2023

DOI: 10.1002/pro.4598

FULL-LENGTH PAPER

THE PROTEIN SOCIETY WILEY

Nanoscale imaging of individual amyloid aggregates extracted from brains of Alzheimer and Parkinson patients reveals presence of lipids in α-synuclein but not in amyloid β_{1-42} fibrils

Kiryl Zhaliazka[1] | **Dmitry Kurouski**[1,2]

[1]Department of Biochemistry and Biophysics, Texas A&M University, College Station, Texas, USA

[2]Department of Biomedical Engineering, Texas A&M University, College Station, Texas, USA

Correspondence
Dmitry Kurouski, Department of Biochemistry and Biophysics, Texas A&M University, College Station, TX 77843, USA.
Email: dkurouski@tamu.edu

Funding information
National Institute of General Medical Sciences, Grant/Award Number: R35GM142869

Review Editor: Aitziber L. Cortajarena

Abstract

Abrupt aggregation of misfolded proteins is the underlying molecular cause of Alzheimer disease (AD) and Parkinson disease (PD). Both AD and PD are severe pathologies that affect millions of people around the world. A small 42 amino acid long peptide, known as amyloid β (Aβ), aggregates in the frontal cortex of AD patients forming oligomers and fibrils, highly toxic protein aggregates that cause progressive neuron death. Similar aggregates of α-synuclein (α-Syn), a small protein that facilitates neurotransmitter release, are observed in the midbrain, hypothalamus, and thalamus of people with PD. In this study, we utilized the innovative nano-Infrared imaging technique to investigate the structural organization of individual Aβ and α-syn fibrils *postmortem* extracted from brains of AD and PD patients, respectively. We observed two morphologically different Aβ and α-Syn fibril polymorphs in each patient's brain. One had twisted topology, whereas another exhibited flat tape-like morphology. We found that both polymorphs shared the same parallel β-sheet-dominated secondary structure. These findings suggested that both fibril polymorphs were built from structurally similar if not identical filaments that coiled forming twisted fibrils or associated side-by-side in the case of straight Aβ and α-Syn fibrils. Nano-Infrared analysis of individual protein aggregates also revealed the presence of lipids in the structure of both twisted and tape-like α-Syn fibrils that were not observed in any of the Aβ fibril polymorphs. These findings demonstrate that lipid membranes can play a critically important role in the onset and progression of PD.

KEYWORDS

AFM-IR, Alzheimer disease, amyloid β_{1-42}, fibrils, oligomers, Parkinson disease, α-synuclein

1 | INTRODUCTION

There are more than 10 million people around the world diagnosed with Parkinson's disease (PD), whereas the number of Alzheimer disease (AD) patients is reaching 40 million (Apetri et al., 2006; Chen et al., 2015; Cremades et al., 2012; Hong et al., 2011; Kurouski et al., 2015; Pieri et al., 2016; Wischik et al., 1985; Wischik et al., 1988). PD is the fastest growing neurodegenerative pathology, projected to strike more than

12 million people by 2040 worldwide. There are 60,000 cases of PD diagnosed annually in the United States, with estimated costs that are upwards of 30 billion, whereas AD is the sixth leading death cause in the United States (Chiti & Dobson, 2017; Iadanza, Jackson, et al., 2018) This makes effective neuroprotective treatments an urgent and unmet need (Chiti & Dobson, 2017).

Although the exact cause of both AD and PD is unclear, these pathologies are strongly associated with an abrupt aggregation of misfolded proteins (Chiti & Dobson, 2017). In the case of AD, 40 and 42 amino acid long amyloid β (Aβ) peptides ($A\beta_{1-40}$ and $A\beta_{1-42}$, respectively) aggregate forming first small prefibrillar oligomers that propagate into amyloid fibrils (Apetri et al., 2006; Chen et al., 2015; Chiti & Dobson, 2017; Cremades et al., 2012; Hong et al., 2011; Iadanza, Jackson, et al., 2018; Kurouski et al., 2015; Pieri et al., 2016). Both oligomers and fibrils were found to be highly toxic to neurons (Chen et al., 2015; Knowles et al., 2014). Solid-state nuclear magnetic resonance and cryo-electron microscopy (cryo-EM) were able to resolve secondary structure of several different $A\beta_{1-40}$ and $A\beta_{1-42}$ fibril polymorphs (Guerrero-Ferreira et al., 2018; Kollmer et al., 2019; Kurouski et al., 2010; Kurouski, Deckert-Gaudig, et al., 2014; Li et al., 2018; Tycko, 2011). Cryo-EM also revealed substantial diversity of amyloid structures, showing that the same protein sequence can adopt different amyloid structures, leading to more fibril structures than sequences (Gallardo et al., 2020; Iadanza, Jackson, et al., 2018). These findings suggested that the morphology of amyloid fibrils is determined by the number and arrangement of protofilaments and the structure of the subunit itself, with variations in these factors potentially affecting the onset and progression of amyloid diseases (Iadanza, Jackson, et al., 2018; Iadanza, Silvers, et al., 2018).

PD is linked to the abrupt aggregation of α-synuclein (α-Syn), a small 14 kDa protein that regulates neurotransmitter release by synaptic vesicles (Auluck et al., 2010; Burré et al., 2010, 2014; Diao et al., 2013). Similar to Aβ, α-Syn aggregation yields small oligomers and fibrils (Hoffmann et al., 2019; Vogiatzi et al., 2008). These toxic protein aggregates are responsible for the onset and spread of PD (Cascella et al., 2021; Colla et al., 2012; Fusco et al., 2017; Yamada & Iwatsubo, 2018). Microscopic examination of Lewy bodies, extracellular formations that appear in the midbrain, hypothalamus, and thalamus upon PD, revealed the presence of lipid membranes together with α-Syn fibrils (Rambaran & Serpell, 2008; Wischik et al., 1985; Wischik et al., 1988). These findings suggested that lipids could be involved in α-Syn aggregation. It was also found that phospholipids, the major constituents of the plasma membrane of neurons, could alter the rates of protein aggregation (Bodner et al., 2009; Bodner et al., 2010; Harayama & Riezman, 2018; Iyer et al., 2016; Musteikytė et al., 2021). Our group demonstrated that phospholipids not only altered the rates of α-Syn aggregation but also uniquely modified the secondary structure of the α-Syn oligomers (Dou et al., 2021a; Dou & Kurouski, 2022). Furthermore, we found that lipids were present in α-Syn oligomers formed at the early stages of protein aggregation together with phosphatidylcholine (PC) and phosphatidylserine (PS; Dou et al., 2021a; Dou & Kurouski, 2022).

These conclusions were made by the direct structural analysis of individual α-Syn oligomers using atomic force microscopy Infrared (AFM-IR) spectroscopy. (Dou et al., 2021a) AFM-IR is an emerging analytical technique that can be used to unravel the secondary structure of analyzed protein specimens (Dazzi & Prater, 2017; Dou et al., 2020; Kurouski et al., 2020). AFM-IR allows for positioning a metalized scanning probe at individual oligomers and fibrils. Next, the probe-sample junction is illuminated by pulsed tunable IR light, which induces thermal expansions in the sample (Katzenmeyer et al., 2013; Kurouski et al., 2020; Strelcov et al., 2017). These thermal expansions are transduced by the scanning probe and converted into IR spectra (Chae et al., 2017; Schwartz et al., 2022), which, in turn, can be used to determine the secondary structure and composition of the analyzed specimens (Dou et al., 2021b; Ramer et al., 2018; Rizevsky & Kurouski, 2020; Ruggeri et al., 2015, 2016, 2018, 2020). Using AFM-IR, Rizevsky et al. (2022) found that PC, PS, and cardiolipin uniquely altered the secondary structure of insulin oligomers and fibrils. Furthermore, these lipids were found to be present in the structure of insulin oligomers. Matveyenka et al. (2022b, 2022d) also found that such oligomers exerted significantly lower cell toxicity than insulin aggregates grown in a lipid-free environment. These results suggest that lipid-determined protein aggregation can be a general phenomenon observed in many if not all amyloid-associated proteins.

In this study, we utilized AFM-IR to examine the secondary structure of individual Aβ and α-Syn fibrils extracted from the brain of different AD and PD patients. In both AD and PD brains, we observed two fibril polymorphs with straight and twisted topologies. We also found that these polymorphs shared a very similar if not identical secondary structure that was dominated by a parallel β-sheet. These results suggested that both polymorphs were grown from similar if not identical filaments that coiled forming twisted fibrils or associated side-by-side in the case of straight Aβ and α-syn fibrils. We also found that the secondary structure of such ex vivo extracted Aβ and α-Syn fibrils were substantially

different from their in vitro grown analogs. Finally, our results revealed the presence of lipids in the structure of both twisted and tape-like α-Syn fibrils that were not observed in any of the analyzed Aβ fibril polymorphs.

2 | RESULTS AND DISCUSSION

Morphological examination of amyloid aggregates extracted from both AD and PD brains revealed the presence of two fibril polymorphs: twisted (T-fibrils) and straight (S-fibrils; Figure 1). Both T-fibril and S-fibril polymorphs had similar dimensions with heights ranging from 6 to 14 nm (Figure S1).

Nanoscale Infrared analysis of Aβ fibrils *postmortem* extracted from the brain of an AD patient revealed that both S-polymorphs and T-polymorphs exhibited IR spectra with peaks at 1694 and 1661–1672 cm^{-1}, Figures 2 and S2. These peaks originated from antiparallel β-sheet and unordered protein secondary structure, respectively (Figure 2a,b; Dou et al., 2021a; Dou & Kurouski, 2022) In the acquired AFM-IR spectra, we also found a peak at 1639 cm^{-1} with a shoulder at 1625 cm^{-1}, which could be assigned to a parallel β-sheet (Matveyenka et al., 2022c, 2022d) Finally, we observed vibrational bands that could be assigned to amino acid side chains (1597–1580 cm^{-1}), as well as amide II vibration of the peptide bond (1550–1500 cm^{-1}; Dou et al., 2020).

Quantitative fitting of acquired AFM-IR spectra revealed that both S-polymorphs and T-polymorphs had similar areas of the discussed above peaks (Figures 2c, S2, and S3). These findings suggested that the secondary structure of both polymorphs was very similar. Specifically, Aβ fibril T-polymorphs were dominated with parallel β-sheet (81%) with a small amount of antiparallel β-sheet (3%) present in their secondary structure. We also found that 16% of protein secondary structure of Aβ fibril T-polymorphs was occupied with unordered protein. Aβ fibril S-polymorphs possessed 84% of parallel and 2% of antiparallel β-sheet with 13% occupied by unordered protein structure, Figure 2c. AFM-IR imaging revealed a uniform distribution of parallel β-sheet, unordered protein secondary structure, and antiparallel β-sheet in both S-polymorphs and T-polymorphs of Aβ fibrils (Figure 2d–o).

We also found that Aβ fibrils extracted from other brains had similar secondary structure to the discussed above S-polymorphs and T-polymorphs. Specifically, the amount of parallel β-sheet in Aβ T-polymorphs extracted from another brain was 83% (Figure S4). These aggregates possessed 2% antiparallel β-sheet and 15% of unordered protein secondary structure. These results suggested that structurally and morphologically similar T-fibril polymorphs were formed in different individuals upon AD. We also found that Aβ S-polymorphs extracted from another brain possessed 82% of parallel and 2% of antiparallel β-sheet together with 16% of unordered protein secondary structure. Thus, one could conclude that the secondary structure of Aβ T-polymorphs remains consistent between different individuals diagnosed with AD.

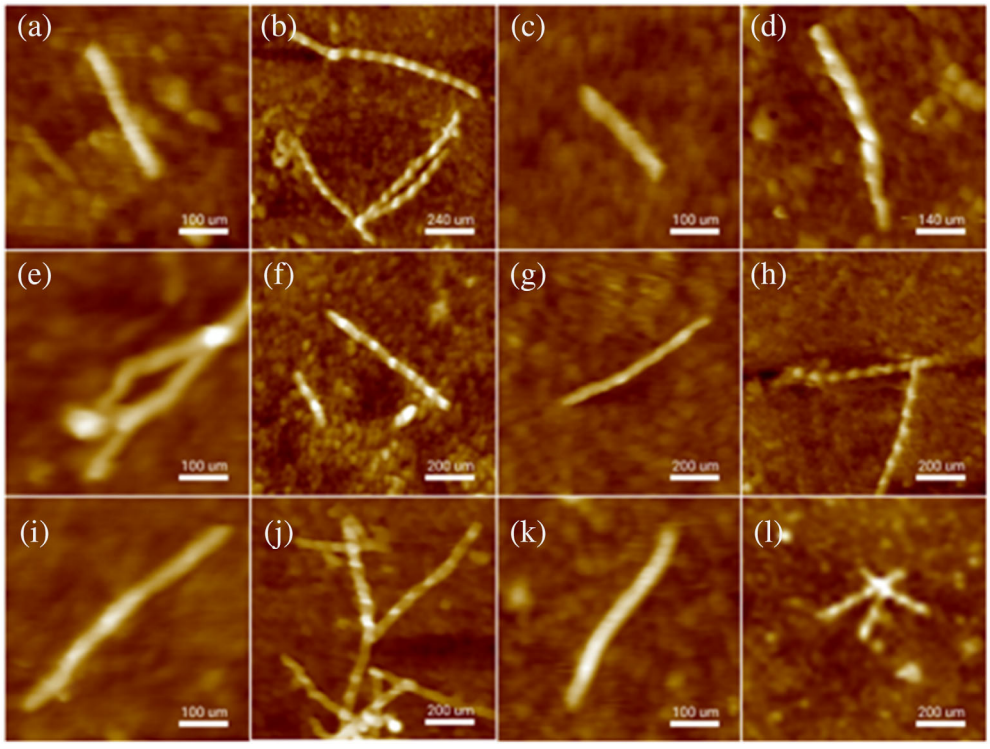

FIGURE 1 Atomic force microscopy images of flat (a,c,e, g,i,k) twisted polymorph (b,d,f, h,j,l) extracted from Alzheimer disease and (a–f) and Parkinson disease (g–l) brains.

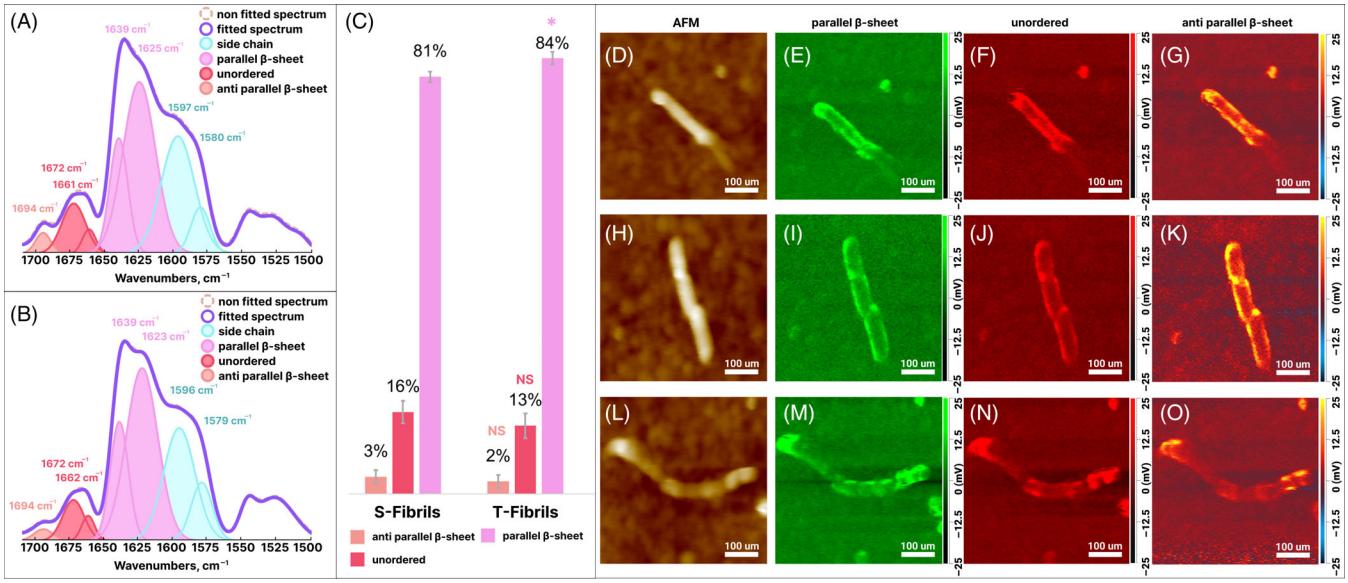

FIGURE 2 Averaged atomic force microscopy Infrared (AFM-IR) spectra acquired from ex vivo amyloid β (Aβ) straight (S-fibril; a) and twisted (T-fibril; b) polymorphs. Histogram (c) of relative contributions of parallel and antiparallel β-sheet and unordered protein. AFM (d,h, l) images of S-fibril (d–g) and T-fibril (h–o) polymorphs with the corresponding nano-IR images that reveal the nanoscale distribution of their parallel β-sheet (1630 cm^{-1}; e,i,m), unordered protein (1667 cm^{-1}; f,j,n) and antiparallel β-sheet (1694 cm^{-1}; g,k,o). Pink asterisk (*) shows statistically significant level of differences between parallel β-sheet secondary structure content of S-fibrils and T-fibrils. *$p \leq 0.05$, Red and orange "NS" demonstrate statistically insignificant differences between unordered and antiparallel β-sheet secondary structure content of S-fibrils and T-fibrils, respectively. ANOVA with Tukey's HSD post hoc test was performed to determine statistical significance of different protein secondary structures.

Nanoscale Infrared analysis of α-Syn aggregates extracted from PD brains revealed a predominance of parallel β-sheet in both T-fibril and S-fibril polymorphs (Figures 3a,b and S5). Specifically, these polymorphs possessed 67% and 63% of parallel β-sheet in their secondary structure, respectively (Figure 3c). We also found that both T-fibril and S-fibril polymorphs had significantly greater amounts of antiparallel β-sheet (10%) in their structure compared with Aβ aggregates (~2.5%). Finally, T-fibril and S-fibril polymorphs of α-Syn possessed 23% and 27% of unordered secondary structure, respectively. This was significantly greater than the amount of unordered secondary structure present in the corresponding Aβ aggregates. It should be noted that similar to Aβ fibrils, we observed a relatively uniform distribution of parallel β-sheet (1630 cm^{-1}), unordered protein (1667 cm^{-1}), and antiparallel β-sheet (1694 cm^{-1}) in both T-fibril and S-fibril polymorphs of α-Syn fibrils (Figure 3d–o). Finally, we observed a vibrational band in the AFM-IR spectra collected from both fibril polymorphs of α-Syn centered ~1728 cm^{-1} (Figure 3a,b; Matveyenka et al., 2022a; 2022c, 2022d; Zhaliazka & Kurouski, 2023). This vibrational band originates from the carbonyl vibration of lipids. We also utilized matrix-assisted laser desorption/ionization (MALDI) to confirm presence of lipids in the analyzed samples. MALDI revealed presence of phosphatidylinositol, phosphatidylethanolamine, PC, PS, and other lipids the analyzed samples (Figure S6 and Table S1). Therefore, we can conclude that in vivo formed α-Syn fibrils possess lipids in their structure. This conclusion is in good agreement with the experimental results reported by Dou et al. (2021a) and Dou & Kurouski (2022) that demonstrated the presence of lipids in α-Syn oligomers grown in the presence of PC and PS.

Similar distributions of the discussed above protein secondary structures were obtained in α-Syn fibrils extracted from two other PD brains. Specifically, we found ~1728 cm^{-1} band in AFM-IR spectra collected from both T-fibril and S-fibril polymorphs of α-Syn fibrils (Figure S5). These polymorphs exhibited 66% of parallel and 11% of antiparallel β-sheet together with 23% of unordered protein secondary structure. Based on these results, we could conclude that T-fibril and S-fibril polymorphs of α-Syn fibrils had similar if not an identical secondary structure that was conserved between different PD patients.

These results are in good agreement with experimental findings reported by Nafie and Lednev groups for insulin and lysozyme aggregates (Kurouski et al., 2010, 2012; Kurouski, Lu, et al., 2014). Using vibrational circular dichroism and AFM, Kurouski, Lu, et al., 2014

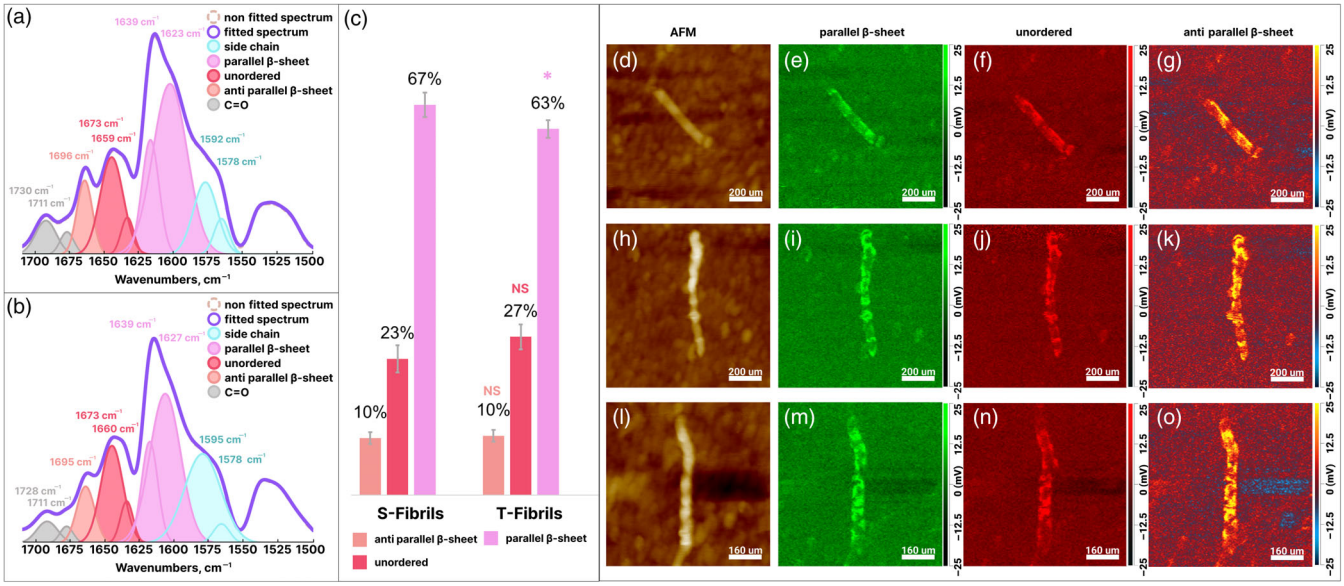

FIGURE 3 Averaged atomic force microscopy Infrared (AFM-IR) spectra acquired from ex vivo α-synuclein (α-Syn) straigh (S-fibril; a) and twisted (T-fibril; b) polymorphs. Histogram (c) of relative contributions of parallel and antiparallel β-sheet and unordered protein. AFM (d,h,l) images of S-fibril (d–g) and T-fibril (h–o) polymorphs with the corresponding nano-IR images that reveal the nanoscale distribution of their parallel β-sheet (1630 cm^{-1}; e,i,m), unordered protein (1667 cm^{-1}; f,j,n) and antiparallel β-sheet (1694 cm^{-1}; g,k,o). Pink asterisk (*) shows statistically significant level of differences between parallel β-sheet secondary structure content of S-fibrils and T-fibrils. *$p \leq 0.05$, Red and orange "NS" demonstrate statistically insignificant differences between unordered and antiparallel β-sheet secondary structure content of S-fibrils and T-fibrils, respectively. ANOVA with Tukey's HSD post hoc test was performed to determine statistical significance of different protein secondary structures.

showed that T-insulin and S-insulin, and lysozyme fibrils were composed of the same filaments that were coiling and breading in the case of T-fibrils and associating side-by-side to form S-fibrils. Expanding upon this, we could conclude that both T-polymorphs and S-polymorphs of Aβ fibrils were built up from the same filaments that were coiling to form T-fibrils and associated side by side with other filaments to make S-fibril polymorphs. Our results also showed that similar processes took place in the case of α-Syn aggregation. Specifically, both T-fibril and S-fibril polymorphs of α-Syn were built from the same filaments that were coiling or associating side by side to develop T-fibril and S-fibril polymorphs, respectively.

The question to ask is whether in vitro aggregation of both Aβ and α-Syn would yield morphologically, and structurally similar protein aggregates compared with those formed in vivo. To answer this question, we aggregated both Aβ and α-Syn in vitro under commonly used experimental conditions (Chen et al., 2015; Lomont et al., 2018; Peralvarez-Marin et al., 2008; Sarroukh et al., 2013; Vosough & Barth, 2021). Next, we utilized AFM-IR to examine the morphology and secondary structure of both Aβ and α-Syn aggregates (Figure 4). We found that in vitro Aβ formed fibrils did not have a clearly defined twist. These fibrils possessed a significantly lower amount of parallel β-sheet (68%) compared with ex vivo extracted aggregates (80%). Furthermore, in vitro, Aβ had a significantly higher amount of unordered protein (27%) compared with ex vivo extracted fibrils (16%), while the amount of antiparallel β-sheet was similar (3%–5%) between these two different groups of fibrils.

We also found that in vitro aggregation of α-Syn yielded exclusively T-fibril polymorphs. Specifically, we observed no S-fibrils present in analyzed protein samples. These fibrils possessed a similar amount of parallel β-sheet (68%) compared with ex vivo extracted aggregates (65%). However, in vitro grown α-Syn fibrils had a significantly larger amount of unordered protein secondary structure (34% vs. 24%) and possessed a substantially lower amount of antiparallel β-sheet (2% vs. 10%) compared with ex vivo extracted α-Syn fibrils. We also observed no carbonyl vibration of lipids in the AFM-IR spectra acquired from in vitro grown α-Syn fibrils. These results demonstrated that in vitro experiments may not fully represent processes linked to the aggregation of misfolded proteins that are taken place in the human brain.

Nevertheless, AFM-IR analysis of both in vitro formed and ex vivo extracted amyloid fibrils demonstrated predominance of parallel β-sheet in their secondary structure. These results are in a good agreement with the experimental findings reported by Eisenberg group (Nelson et al., 2005; Nelson & Eisenberg, 2006a, 2006b).

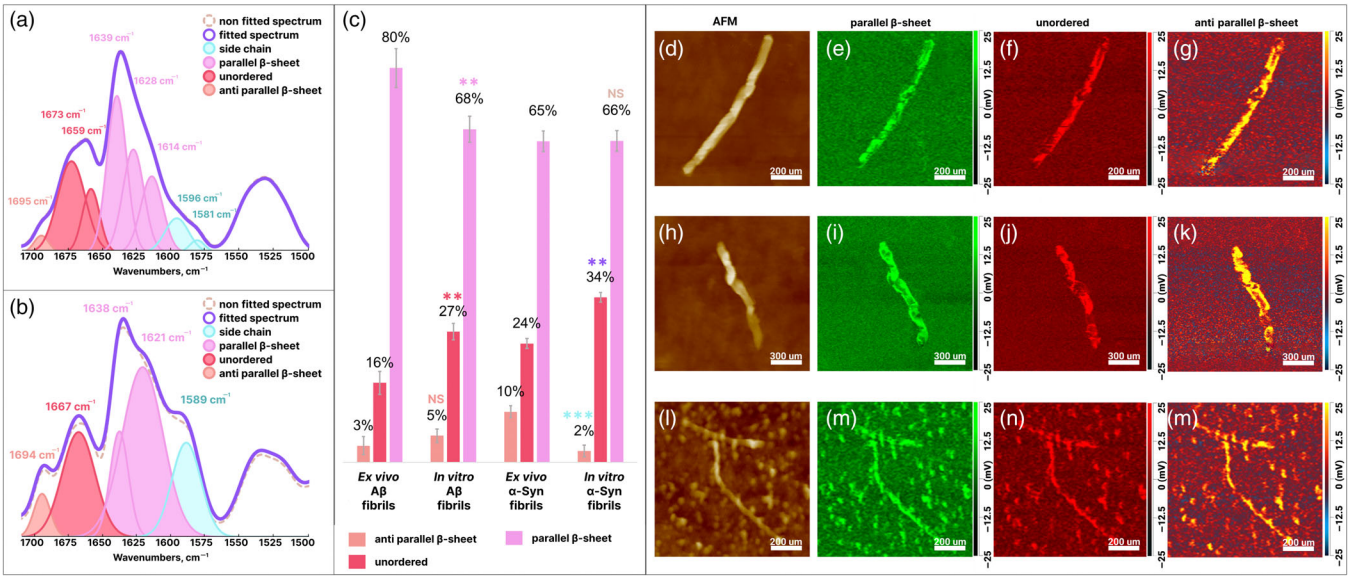

FIGURE 4 Averaged atomic force microscopy Infrared (AFM-IR) spectra acquired from in vitro amyloid β (Aβ) (A) and α-synuclein (α-Syn; b) fibrils. Histogram (c) of relative contributions of parallel and antiparallel β-sheet and unordered protein in ex vivo Aβ and α-Syn, as well as in vitro Aβ and α-Syn fibrils. AFM (d,h,l) images of in vitro Aβ (d–k) and α-Syn (l–o) fibrils with the corresponding nano-IR images that reveal the nanoscale distribution of their parallel β-sheet (e,i,m), unordered protein (f,j,n) and antiparallel β-sheet (g,k,o). Pink and red asterisks (*) show the significance level of differences between parallel β-sheet and unordered secondary structure content of ex vivo and in vitro Aβ fibrils, respectively. Purple and light blue asterisks (*) show the significance level of differences between unordered and antiparallel β-sheet secondary structure content of ex vivo and in vitro α-Syn fibrils, respectively. NS is a nonsignificant difference, and $^{*}p \leq 0.05$, $^{**}p \leq 0.01$, $^{***}p \leq 0.001$. ANOVA with Tukey's HSD post hoc test was performed to determine statistical significance of different protein secondary structures.

X-ray spectroscopy and computational approaches used by Eisenberg demonstrated that cross-β-sheet is the core structure of amyloid aggregates (Eisenberg & Sawaya, 2017a, 2017b; Sangwan et al., 2017).

3 | CONCLUSIONS

Nanoscale structural analysis of protein aggregates extracted from brains of both AD and PD patients revealed presence of two morphologically different fibril polymorphs that have twisted and straight topologies. We found that the secondary structure of T-polymorph and S-polymorph of Aβ fibrils is dominated by parallel β-sheet (∼83%) with some amount of antiparallel β-sheet (2%). We also found that ∼16% of T-polymorph and S-polymorph of Aβ fibrils are occupied by unordered protein secondary structure. Similar to Aβ, the secondary structure of α-Syn T-polymorphs and S-polymorphs is dominated by parallel β-sheet (∼65%) with some amount of antiparallel β-sheet (10%). We also observed around 25% of the secondary structure of both T-polymorphs and S-polymorphs of α-Syn fibrils occupied with unordered protein secondary structure. In the AFM-IR spectra acquired from ex vivo extracted α-Syn fibrils, we also found the vibrational signature of lipids. These results show that lipids are present in the structure of α-Syn fibrils. These findings demonstrate that lipids can be directly involved in α-Syn aggregation. Finally, our results show that in vitro aggregation of both Aβ and α-Syn results in structurally different protein aggregates compared with those extracted from the human brain.

4 | MATERIALS AND METHODS

4.1 | Brain tissue samples

Frontal cortex of three clinically confirmed AD patients (55–65 years) and the midbrain of three PD-confirmed patients (50–80 years) were received from NIH NeuroBioBank. All *postmortem* obtained brain samples were fresh-frozen and were kept at −80°C before the fibril extraction.

4.2 | Fibril extraction

Fibrils were extracted from brain samples using a water extraction protocol. Briefly, 250 mg of tissue material was homogenized with a scalpel and washed five times with 0.5 mL of calcium tris buffer (20 mm Tris, 138 mm NaCl, 2 mm Tris, pH 8.0). During washing steps, gentle stirring

of brain tissue was performed. Next, tissue samples were centrifuged at 3100*g* at 4°C for 1 min. After the supernatant was removed, pellets were re-suspended in 1 mL of freshly made 5 mg/mL *Clostridium histolyticum* collagenase (Sigma-Aldrich, St. Louis, Missouri) in tris calcium buffer. After overnight incubation at 37°C in a horizontal orbital shaker at 750 rpm, tissue samples were again centrifuged at 3100*g* for 30 min at 4°C. The supernatant was discarded. The retained pellets were homogenized in 0.5 mL of tris-ethylenediaminetetraacetic acid (EDTA) buffer (20 mM Tris, 140 mM NaCl, 10 mM EDTA, pH 8.0). After centrifugation for 5 min at 3100*g* and 4°C, the pellet was carefully separated from the supernatant. The pellet was homogenized in 0.5 mL of ice-cold water and centrifuged at 3100*g* for 5 min at 4°C. After centrifugation supernatant contain extracted fibrils sample.

4.3 | Dot western blotting

Dot western blotting was performed to confirm the presence of Aβ and α-Syn aggregates in extracted brain material using the Bio-Dot Microfiltration Apparatus (Bio-Rad, cat. No. 170–6545), as illustrated in Figure S7. The nitrocellulose membrane (Bio-Rad, cat. No. 1620117) was rehydrated with 100 μL of TBS buffer (pH 7.4) prior to adding 200 μL of sample to each well. The samples were incubated on the membrane for 60 min before being drained from the apparatus. The membrane was then blocked with 300 μL of 5% nonfat dry milk in 1×TBS solution for 60 min, followed by two wash steps with 300 μL of 1×TBS/Tween pH 7.6 (Bio-Rad, cat. No. BUF028). Primary antibodies (Invitrogen Anti-β Amyloid (Apetri et al., 2006; Auluck et al., 2010; Bodner et al., 2009, 2010; Burré et al., 2010, 2014; Cascella et al., 2021; Chae et al., 2017; Chen et al., 2015; Chiti & Dobson, 2017; Colla et al., 2012; Cremades et al., 2012; Dazzi & Prater, 2017; Diao et al., 2013; Dou et al., 2020, 2021a, 2021b; Dou & Kurouski, 2022; Eisenberg & Sawaya, 2017a, 2017b; Fusco et al., 2017; Gallardo et al., 2020; Guerrero-Ferreira et al., 2018; Harayama & Riezman, 2018; Hoffmann et al., 2019; Hong et al., 2011; Iadanza, Jackson, et al., 2018; Iadanza, Silvers, et al., 2018; Iyer et al., 2016; Katzenmeyer et al., 2013; Knowles et al., 2014; Kollmer et al., 2019; Kurouski et al., 2010, 2012, 2015, 2020; Kurouski, Deckert-Gaudig, et al., 2014; Kurouski, Lu, et al., 2014; Li et al., 2018; Lomont et al., 2018; Matveyenka et al., 2022a, 2022b) Monoclonal (GT622), Catalog no. MA5-36246; Millipore Ms X α-Syn, cat. no. MAB5320) were added to the wells at a final dilution ratio of 1:1000, followed by gravity filtration and three wash steps with 300 μL of 1×TBS/Tween pH 7.6. Secondary antibodies (Invitrogen Goat Anti-Mouse IgG [H + L] DyLight 633 Conjugated, Ref 355,512) were added with a final dilution ratio of 1:1000, followed by two wash steps with 300 μL of 1×TBS/Tween pH 7.6. The membrane was then removed, dried for 5 min and imaged using the Amersham Imager 600 Western Blot Imager (Amersham, UK).

4.4 | Protein aggregation

One milligram of human $A\beta_{1-42}$ (Gene script Cat. no. RP10017) was dissolved in 1 mL of HFIP (Across organics, code 445820500). After the peptide was fully dissolved, HFIP was evaporated under the N_2 stream. The resulting protein film was dissolved in 6 M guanidine chloride at 4°C. Next, 6 M guanidine chloride was replaced with 20 mM PB pH 7.4 using a PD-10 desalting column (Cytiva, Cat. no. 17085101) at 4°C to suppress peptide aggregation. The final sample contained 60 μM of $A\beta_{1-42}$. The sample was incubated at 25°C under quiescent conditions for 48 h. In parallel, human recombinant α-Syn (Anaspec, cat. no. AS-55555-1000) was dissolved in 20 mM PB pH 7.4 to obtain a 150 μM final concentration of the protein. Samples were incubated at 37°C, 750 rpm agitation for 5 days.

4.5 | Atomic force microscopy Infrared

Solutions (150 μL) of brain extracts and in vitro-prepared protein aggregates in 20 mM PB pH 7.4 buffer were placed on silicon wafers. After ~3 min of sample exposure on a silicon surface, wafers were rinsed with DI water and dried at room temperature. Nano-IR3 system equipped with a QCL laser was used for AFM-IR imaging and spectral acquisition (Bruker, Santa Barbara, California). Spectral resolution was 2 cm^{-1}/pt; laser sweeping speed was 230 kHz, and laser repletion rate was 3.12%. No PLL was used for sample imaging. All spectra and maps were obtained using contact-mode AFM tips (ContGB-G AFM probe, NanoAndMore). In Analysis Studio 3.15, all raw spectra were smoothed with a 10-point filter and then normalized by average area. Spectra were fitted using GRAMS/AI™ Spectroscopy Software. ANOVA ($p < 0.05$) with Tukey's HSD post hoc test was used to determine statistical significance of the differences between in vitro and ex vivo Aβ and αSyn fibrils.

4.6 | Matrix-assisted laser desorption/ionization

Bruker ultraflextreme MALDI-TOF-TOF instrument was used for analysis of lipids present in brain extract. For performed experiments, 2,5-dihydroxybenzoic acid

matrix prepared in 50% acetonitrile and 0.1% formic acid was used.

AUTHOR CONTRIBUTIONS

Kiryl Zhaliazka: Conceptualization (lead); data curation (lead); formal analysis (lead); investigation (lead); methodology (lead). **Dmitry Kurouski:** Conceptualization (lead); resources (lead); supervision (lead); writing – original draft (lead).

ACKNOWLEDGMENTS

We are grateful to the National Institute of Health for the provided financial support (R35GM142869). We are grateful to. Gayan I. Nawaratna from Protein Chemistry Lab for the help with MALDI analysis of extracted protein aggregates.

CONFLICT OF INTEREST STATEMENT

The authors declare no competing financial interests.

ORCID

Dmitry Kurouski https://orcid.org/0000-0002-6040-4213

REFERENCES

Apetri MM, Maiti NC, Zagorski MG, Carey PR, Anderson VE. Secondary structure of alpha-synuclein oligomers: characterization by raman and atomic force microscopy. J Mol Biol. 2006;355:63–71.

Auluck PK, Caraveo G, Lindquist S. α-Synuclein: membrane interactions and toxicity in Parkinson's disease. Annu Rev Cell Develop Biol. 2010;26:211–33.

Bodner CR, Dobson CM, Bax A. Multiple tight phospholipid-binding modes of α-synuclein revealed by solution NMR spectroscopy. J Mol Biol. 2009;390:775–90.

Bodner CR, Maltsev AS, Dobson CM, Bax A. Differential phospholipid binding of α-synuclein variants implicated in Parkinson's disease revealed by solution NMR spectroscopy. Biochemistry. 2010;49:862–71.

Burré J, Sharma M, Südhof TC. α-Synuclein assembles into higher-order multimers upon membrane binding to promote SNARE complex formation. Proc Natl Acad Sci U S A. 2014;111:E4274–83.

Burré J, Sharma M, Tsetsenis T, Buchman V, Etherton MR, Südhof TC. Alpha-synuclein promotes SNARE-complex assembly in vivo and in vitro. Science. 2010;329:1663–7.

Cascella R, Chen SW, Bigi A, Camino JD, Xu CK, Dobson CM, et al. The release of toxic oligomers from α-synuclein fibrils induces dysfunction in neuronal cells. Nat Commun. 2021;12:1814.

Chae J, An S, Ramer G, Stavila V, Holland G, Yoon Y, et al. Nanophotonic atomic force microscope transducers enable chemical composition and thermal conductivity measurements at the nanoscale. Nano Lett. 2017;17:5587–94.

Chen SW, Drakulic S, Deas E, Ouberai M, Aprile FA, Arranz R, et al. Structural characterization of toxic oligomers that are kinetically trapped during alpha-synuclein fibril formation. Proc Natl Acad Sci U S A. 2015;112:E1994–2003.

Chiti F, Dobson CM. Protein misfolding, amyloid formation, and human disease: a summary of Progress over the last decade. Annu Rev Biochem. 2017;86:27–68.

Colla E, Jensen PH, Pletnikova O, Troncoso JC, Glabe C, Lee MK. Accumulation of toxic α-synuclein oligomer within endoplasmic reticulum occurs in α-synucleinopathy in vivo. J Neurosci. 2012;32:3301–5.

Cremades N, Cohen SI, Deas E, Abramov AY, Chen AY, Orte A, et al. Direct observation of the interconversion of normal and toxic forms of alpha-synuclein. Cell. 2012;149:1048–59.

Dazzi A, Prater CB. AFM-IR: technology and applications in nanoscale infrared spectroscopy and chemical imaging. Chem Rev. 2017;117:5146–73.

Diao J, Burré J, Vivona S, Cipriano DJ, Sharma M, Kyoung M, et al. Native α-synuclein induces clustering of synaptic-vesicle mimics via binding to phospholipids and synaptobrevin-2/VAMP2. Elife. 2013;2:e00592.

Dou T, Kurouski D. Phosphatidylcholine and phosphatidylserine uniquely modify the secondary structure of alpha-synuclein oligomers formed in their presence at the early stages of protein aggregation. ACS Chem Nerosci. 2022;13:2380–5.

Dou T, Li Z, Zhang J, Evilevitch A, Kurouski D. Nanoscale structural characterization of individual viral particles using atomic force microscopy infrared spectroscopy (AFM-IR) and tip-enhanced Raman spectroscopy (TERS). Anal Chem. 2020;92:11297–304.

Dou T, Zhou L, Kurouski D. Unravelling the structural organization of individual alpha-synuclein oligomers grown in the presence of phospholipids. J Phys Chem Lett. 2021a;12:4407–14.

Dou T, Zhou L, Kurouski D. Unravelling the structural Organization of Individual α-synuclein oligomers grown in the presence of phospholipids. J Phys Chem Lett. 2021b;12:4407–14.

Eisenberg DS, Sawaya MR. Neurodegeneration: taming tangled tau. Nature. 2017a;547:170–1.

Eisenberg DS, Sawaya MR. Structural studies of amyloid proteins at the molecular level. Annu Rev Biochem. 2017b;86:69–95.

Fusco G, Chen SW, Williamson PTF, Cascella R, Perni M, Jarvis JA, et al. Structural basis of membrane disruption and cellular toxicity by α-synuclein oligomers. Science. 2017;358:1440–3.

Gallardo R, Ranson NA, Radford SE. Amyloid structures: much more than just a cross-beta fold. Curr Opin Struct Biol. 2020;60:7–16.

Guerrero-Ferreira R, Taylor NM, Mona D, Ringler P, Lauer ME, Riek R, et al. Cryo-EM structure of alpha-synuclein fibrils. Elife. 2018;7:e36402.

Harayama T, Riezman H. Understanding the diversity of membrane lipid composition. Nat Rev Mol Cell Biol. 2018;19:281–96.

Hoffmann AC, Minakaki G, Menges S, Salvi R, Savitskiy S, Kazman A, et al. Extracellular aggregated alpha synuclein primarily triggers lysosomal dysfunction in neural cells prevented by trehalose. Sci Rep. 2019;9:544.

Hong DP, Han S, Fink AL, Uversky VN. Characterization of the non-fibrillar alpha-synuclein oligomers. Prot Pept Lett. 2011;18:230–40.

Iadanza MG, Jackson MP, Hewitt EW, Ranson NA, Radford SE. A new era for understanding amyloid structures and disease. Nat Rev Mol Cell Biol. 2018;19:755–73.

Iadanza MG, Silvers R, Boardman J, Smith HI, Karamanos TK, Debelouchina GT, et al. The structure of a beta(2)-

microglobulin fibril suggests a molecular basis for its amyloid polymorphism. Nat Commun. 2018;9:4517.
Iyer A, Roeters SJ, Schilderink N, Hommersom B, Heeren RMA, Woutersen S, et al. The impact of N-terminal acetylation of α-synuclein on phospholipid membrane binding and fibril structure. J Biol Chem. 2016;291:21110–22.
Katzenmeyer AM, Aksyuk V, Centrone A. Nanoscale infrared spectroscopy: improving the spectral range of the photothermal induced resonance technique. Anal Chem. 2013;85:1972–9.
Knowles TP, Vendruscolo M, Dobson CM. The amyloid state and its association with protein misfolding diseases. Nat Rev. 2014; 15:384–96.
Kollmer M, Close W, Funk L, Rasmussen J, Bsoul A, Schierhorn A, et al. Cryo-EM structure and polymorphism of Abeta amyloid fibrils purified from Alzheimer's brain tissue. Nat Commun. 2019;10:4760.
Kurouski D, Dazzi A, Zenobi R, Centrone A. Infrared and Raman chemical imaging and spectroscopy at the nanoscale. Chem Soc Rev. 2020;49:3315–47.
Kurouski D, Deckert-Gaudig T, Deckert V, Lednev IK. Surface characterization of insulin protofilaments and fibril polymorphs using tip-enhanced Raman spectroscopy (TERS). Biophys J. 2014;106:263–71.
Kurouski D, Dukor RK, Lu X, Nafie LA, Lednev IK. Spontaneous inter-conversion of insulin fibril chirality. Chem Commun. 2012;48:2837–9.
Kurouski D, Lombardi RA, Dukor RK, Lednev IK, Nafie LA. Direct observation and pH control of reversed supramolecular chirality in insulin fibrils by vibrational circular dichroism. Chem Commun. 2010;46:7154–6.
Kurouski D, Lu X, Popova L, Wan W, Shanmugasundaram M, Stubbs G, et al. Is supramolecular filament chirality the underlying cause of major morphology differences in amyloid fibrils? J Am Chem Soc. 2014;136:2302–12.
Kurouski D, Van Duyne RP, Lednev IK. Exploring the structure and formation mechanism of amyloid fibrils by Raman spectroscopy: a review. Analyst. 2015;140:4967–80.
Li B, Ge P, Murray KA, Sheth P, Zhang M, Nair G, et al. Cryo-EM of full-length alpha-synuclein reveals fibril polymorphs with a common structural kernel. Nat Commun. 2018;9:3609.
Lomont JP, Rich KL, Maj M, Ho JJ, Ostrander JS, Zanni MT. Spectroscopic signature for stable beta-amyloid fibrils versus beta-sheet-Rich oligomers. J Phys Chem B. 2018;122:144–53.
Matveyenka M, Rizevsky S, Kurouski D. Amyloid aggregates exert cell toxicity causing irreversible damages in the endoplasmic reticulum. Biochim Biophys Acta Mol Basis Dis. 2022a;1868:166485.
Matveyenka M, Rizevsky S, Kurouski D. The degree of unsaturation of fatty acids in phosphatidylserine alters the rate of insulin aggregation and the structure and toxicity of amyloid aggregates. FEBS Lett. 2022b;596:1424–33.
Matveyenka M, Rizevsky S, Kurouski D. Length and unsaturation of fatty acids of phosphatidic acid determines the aggregation rate of insulin and modifies the structure and toxicity of insulin aggregates. ACS Chem Nerosci. 2022c;13:2483–9.
Matveyenka M, Rizevsky S, Kurouski D. Unsaturation in the fatty acids of phospholipids drastically alters the structure and toxicity of insulin aggregates grown in their presence. J Phys Chem Lett. 2022d;13:4563–9.
Musteikytė G, Jayaram AK, Xu CK, Vendruscolo M, Krainer G, Knowles TPJ. Interactions of α-synuclein oligomers with lipid membranes. Biochim Biophys Acta Biomembran. 2021;1863: 183536.
Nelson R, Eisenberg D. Recent atomic models of amyloid fibril structure. Curr Opin Struct Biol. 2006a;16:260–5.
Nelson R, Eisenberg D. Structural models of amyloid-like fibrils. Adv Protein Chem. 2006b;73:235–82.
Nelson R, Sawaya MR, Balbirnie M, Madsen AO, Riekel C, Grothe R, et al. Structure of the cross-beta spine of amyloid-like fibrils. Nature. 2005;435:773–8.
Peralvarez-Marin A, Barth A, Graslund A. Time-resolved infrared spectroscopy of pH-induced aggregation of the Alzheimer Abeta(1-28) peptide. J Mol Biol. 2008;379:589–96.
Pieri L, Madiona K, Melki R. Structural and functional properties of prefibrillar α-synuclein oligomers. Sci Rep. 2016;6:24526.
Rambaran RN, Serpell LC. Amyloid fibrils: abnormal protein assembly. Prion. 2008;2:112–7.
Ramer G, Ruggeri FS, Levin A, Knowles TPJ, Centrone A. Determination of polypeptide conformation with nanoscale resolution in water. ACS Nano. 2018;12:6612–9.
Rizevsky S, Kurouski D. Nanoscale structural organization of insulin fibril polymorphs revealed by atomic force microscopy-infrared spectroscopy (AFM-IR). Chembiochem. 2020;21:481–5.
Rizevsky S, Matveyenka M, Kurouski D. Nanoscale structural analysis of a lipid-driven aggregation of insulin. J Phys Chem Lett. 2022;10:2467–73.
Ruggeri FS, Benedetti F, Knowles TPJ, Lashuel HA, Sekatskii S, Dietler G. Identification and nanomechanical characterization of the fundamental single-strand protofilaments of amyloid alpha-synuclein fibrils. Proc Natl Acad Sci U S A. 2018;115: 7230–5.
Ruggeri FS, Flagmeier P, Kumita JR, Meisl G, Chirgadze DY, Bongiovanni MN, et al. The influence of pathogenic mutations in alpha-synuclein on biophysical and structural characteristics of amyloid fibrils. ACS Nano. 2020;14:5213–22.
Ruggeri FS, Longo G, Faggiano S, Lipiec E, Pastore A, Dietler G. Infrared nanospectroscopy characterization of oligomeric and fibrillar aggregates during amyloid formation. Nat Commun. 2015;6:7831.
Ruggeri FS, Vieweg S, Cendrowska U, Longo G, Chiki A, Lashuel HA, et al. Nanoscale studies link amyloid maturity with polyglutamine diseases onset. Sci Rep. 2016;6:31155.
Sangwan S, Zhao A, Adams KL, Jayson CK, Sawaya MR, Guenther EL, et al. Atomic structure of a toxic, oligomeric segment of SOD1 linked to amyotrophic lateral sclerosis (ALS). Proc Natl Acad Sci U S A. 2017;114:8770–5.
Sarroukh R, Goormaghtigh E, Ruysschaert JM, Raussens V. ATR-FTIR: a "rejuvenated" tool to investigate amyloid proteins. Biochim Biophys Acta. 2013;1828:2328–38.
Schwartz JJ, Jakob DS, Centrone A. A guide to nanoscale IR spectroscopy: resonance enhanced transduction in contact and tapping mode AFM-IR. Chem Soc Rev. 2022;51:5248–67.
Strelcov E, Dong Q, Li T, Chae J, Shao Y, Deng Y, et al. CH3NH3PbI3 perovskites: Ferroelasticity revealed. Sci Adv. 2017;3:e1602165.
Tycko R. Solid-state NMR studies of amyloid fibril structure. Annu Rev Phys Chem. 2011;62:279–99.
Vogiatzi T, Xilouri M, Vekrellis K, Stefanis L. Wild type alpha-synuclein is degraded by chaperone-mediated autophagy and macroautophagy in neuronal cells. J Biol Chem. 2008;283: 23542–56.

Vosough F, Barth A. Characterization of homogeneous and heterogeneous amyloid-beta42 oligomer preparations with biochemical methods and infrared spectroscopy reveals a correlation between infrared Spectrum and oligomer size. ACS Chem Neurosci. 2021;12:473–88.

Wischik CM, Crowther RA, Stewart M, Roth M. Subunit structure of paired helical filaments in Alzheimer's disease. J Cell Biol. 1985;100:1905–12.

Wischik CM, Novak M, Thogersen HC, Edwards PC, Runswick MJ, Jakes R, et al. Isolation of a fragment of tau derived from the core of the paired helical filament of Alzheimer disease. Proc Natl Acad Sci U S A. 1988;85:4506–10.

Yamada K, Iwatsubo T. Extracellular α-synuclein levels are regulated by neuronal activity. Mol Neurodegener. 2018;13:9.

Zhaliazka K, Kurouski D. Lipids uniquely alter the secondary structure and toxicity of amyloid beta 1-42 aggregates. FEBS J. 2023. https://doi.org/10.1111/febs.16738

SUPPORTING INFORMATION

Additional supporting information can be found online in the Supporting Information section at the end of this article.

How to cite this article: Zhaliazka K, Kurouski D. Nanoscale imaging of individual amyloid aggregates extracted from brains of Alzheimer and Parkinson patients reveals presence of lipids in α-synuclein but not in amyloid β_{1-42} fibrils. Protein Science. 2023;32(4):e4598. https://doi.org/10.1002/pro.4598